ISDB-T Based Passive Bistatic Radar Testbed

Julian Polimeni
Dpto. Electrotecnia
Fac. de Ingeniería, UNLP
La Plata, Argentina
julian.polimeni@ing.unlp.edu.ar

Juan I. Fernandez Michelli
Dpto. Electrotecnia
Fac. de Ingeniería, UNLP
La Plata, Argentina
jfernandez@ing.unlp.edu.ar

Martin Hurtado
Dpto. Electrotecnia
Fac. de Ingeniería, UNLP
La Plata, Argentina
martin.hurtado@ing.unlp.edu.ar

Carlos Muravchik
Dpto. Electrotecnia
Fac. de Ingeniería, UNLP
La Plata, Argentina
carlosm@ing.unlp.edu.ar

***Abstract*—This paper presents the implementation of a Passive Bistatic Radar (PBR) testbed that exploits the Integrated Services Digital Broadcasting Terrestrial (ISDB-T) signal, a standard operating in South America and Japan, as an illuminator of opportunity. The system is characterized, and its performance is analyzed. Real experimental results are presented and compared with flight data services, demonstrating the effectiveness of the system.**

***Index Terms*—passive bistatic radar, target detection, experimental study.**

I. Introduction

Passive radars are a class of bistatic radar that exploits non-cooperative sources of radio energy as illuminators of opportunity to detect and track targets of interest [1]. Based on the bistatic geometry, passive radar has separated transmitting and receiving antennas. Unlike active radar systems, passive ones do not require a dedicated transmitter, significantly reducing the cost of operation and production. Passive radars offer several advantages, such as utilizing frequency bands not typically available for radar, enabling stealthy target detection and displaying versatility with various opportunity transmissions. However, waveform optimization and signal processing pose challenges, and transmit source control is very limited. Despite these drawbacks, passive radar's cost-effectiveness and broad coverage from existing transmitters make it an appealing technology. [2]

Many broadcast and communication signals have been considered and analyzed as potential passive radar sources. Digital terrestrial television broadcasting (DTTB) signals are particularly attractive due to their wide bandwidth, high radiated power, and well-defined ambiguity function. Since these signals operate in UHF bands, the system implementation is based on available Software Defined Radio (SDR) hardware, specifically Universal Software Radio Peripherals (USRPs). These USRPs are equipped with receiver daughterboards capable of sampling signals within a broad and high-frequency range.

We show an implementation of a PBR system exploiting an ISDB-T signal source and using the USRP-Ettus x300. A similar attempt using DVB-T signal has been presented in [3].

II. Theory

A. Bistatic Geometry

Figure 1 illustrates a two-dimensional representation of the bistatic geometry using Cartesian coordinates. A target is positioned at $[x(t), y(t), z(t)]^T$, while the transmitter and receiver are located at $[x_t, y_t, z_t]^T$ and $[x_r, y_r, z_r]^T$, respectively. The latter are separated by the baseline L, and the angle subtended between them is the bistatic angle β. The range from the transmitter to the target is the target range R_T, and the range from the target to the receiver is the receiver range, R_R. These can be calculated as follows:

$$R_T(t) = \sqrt{(x(t)-x_t)^2 + (y(t)-y_t)^2 + (z(t)-z_t)^2} \quad (1)$$

$$R_R(t) = \sqrt{(x(t)-x_r)^2 + (y(t)-y_r)^2 + (z(t)-z_r)^2} \quad (2)$$

$$L = \sqrt{(x_t-x_r)^2 + (y_t-y_r)^2 + (z_t-z_r)^2} \quad (3)$$

The difference between the indirect path $R_R(t) + R_T(t)$ and the direct path L is called the Bistatic Range $R_B(t)$.

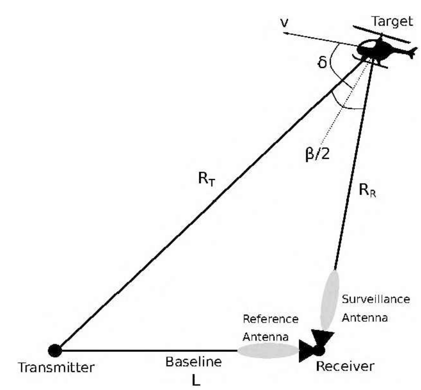

Fig. 1. The PBR geometry

The magnitude of the target velocity projected onto the bistatic plane is represented by V, and its aspect angle is referenced to the bistatic bisector $\beta/2$. The Bistatic Velocity $V_B(t)$, defined as the time derivative of the bistatic range, is given by the following equation:

$$V_B(t) = \frac{dR_B(t)}{dt} = 2V\cos(\delta)\cos(\beta/2) \quad (4)$$

B. Bistatic Radar Equation

The bistatic radar equation defines the basis for a detection performance analysis. It allows calculation of the expected Signal to Noise Ratio (SNR) as a function of target position and radar cross section (RCS), as well as transmitter and receiver characteristics.

ISBN: 978-950-766-230-0

The received power from the target is given by the bistatic equation (5)

$$P_S = P_T G_T \frac{\sigma_B}{4\pi R_T^2} \frac{A_e}{4\pi R_R^2} = P_T G_T \frac{\sigma_B}{4\pi R_T^2} \frac{G_R \lambda^2}{(4\pi)^2 R_R^2} \tag{5}$$

where, the power and antenna gain of the transmitter are denoted as P_T and G_T, respectively. Then, G_R and A_e represent the gain and effective aperture of the receiver antenna, while the target RCS is symbolized as σ_B and λ expresses the carrier wavelength of the opportunity signal.

The target echo signal competes with both the strong direct signal from the transmitter and thermal noise. Taking into account the noise power P_N, the target echo SNR can be calculated as follows:

$$\text{SNR} = \frac{P_S}{P_N} = \frac{P_T G_T \sigma_B G_R \lambda^2}{(4\pi)^3 R_R^2 R_T^2} \frac{1}{\kappa T_0 F_n \Delta B_R} G_{int} \tag{6}$$

where κ is the Boltzmann constant, T_0 is the reference noise temperature, B_R is the bandwidth of the receiver, and F_n is the system noise figure. SNR is increased by the processing gain G_{int} resulting from the correlation of the signal with bandwidth B over time T. The ovals of Cassini [1] are contours where SNR and the range product $R_T R_R$ are held constant. This concept provides an estimate of the bistatic radar coverage.

C. Theory of Operation

Signals emitted from the transmitter can reach the receiver antenna of the radar through different paths. Since the illuminating signal is not a priori known, it has to be measured. Besides the propagation losses, the difference between the lag of the direct path signal and the reflected signal is denoted by τ. The bistatic range $R_B(t)$ is calculated from the measured τ and the speed of light c as:

$$R_B(t) = \tau c \tag{7}$$

The signal reflected from a moving target will also experience the effect of Doppler shift, which depends on the speed and geometry of the aircraft. It is denoted by f_d. The bistatic velocity $V_B(t)$ can be calculated from the measured Doppler shift f_d and the wavelength λ as:

$$V_B(t) = -\lambda f_d \tag{8}$$

Thus, the detection and estimation in passive radar are carried out using of the correlation of the reference and echo signals by way of the cross-ambiguity function (CAF) [4].

$$\Psi(\tau, f_d) = \int_0^{T_{int}} s(t) r^*(t-\tau) e^{-j2\pi f_d t} dt \tag{9}$$

This function is calculated in digital domain and can be written as:

$$\Psi[m,k] = \sum_{n=0}^{N-1} s[n] r^*[n-m] e^{-j\frac{2\pi}{N}kn} \tag{10}$$

where m is an integer corresponding to a signal delay in samples, k is the (integer) number of bins (of the acquisition system) the received frequency is shifted from the carrier frequency, and N is the number of samples of the coherent processing interval (CPI) i.e., $T_{int} = N/f_s$, where f_s is the sampling frequency. The result is a two-dimensional range-velocity matrix (also known as delay-doppler map).

D. USRP Ettus x300

The USRP X300 is an SDR from Ettus Research, a National Instruments company. The device count with high ADC processing bandwidth, i.e. sampling frequency, and the use of Ethernet interface. A simplified system diagram is shown in Figure 2 , depicting the principal functionality of the SDRs. The RF front-end, allows for both receiving, and transmitting operation because the LOs in both chains operate independently. The RF switches in the front-end also permit half-duplex operation on the transmitter port. This allows for a number of different possible antenna configurations.

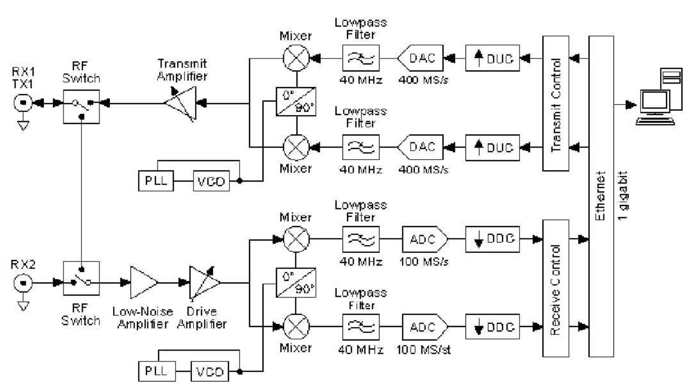

Fig. 2. General USRP architecture [5]

The manufacturer advises considering several factors to ensure channel phase coherence, including the existence of a random phase offset between any two front-ends, variations in phase offset depending on the LO frequencies used, and the possibility of drift in phase offset over time due to thermal factors. To address these challenges, it is recommended to use "timed_commands", a software tool that enables the simultaneous tuning of multiple front-ends, ensuring that the phase offsets between VCO/PLL chains remain constant after each re-tuning. Therefore, periodic calibration will be necessary to effectively maintain phase coherence.

E. Opportunity Signal

The ISDB-T is the standard of Digital TV used in Argentina. It can provide reliable high-quality video, sound, and data broadcasting for fixed and mobile receivers [6]. It offers three transmission modes to accommodate a wide range of transmitting frequencies. In La Plata, the signals are allocated to the 473-605 MHz ultra high frequency (UHF) band. The modulation scheme used is Band Segmented Transmission-Orthogonal Frequency Division Multiplexing (BST-OFDM), which consists of a set of common basic frequency blocks called BST segments. Each ISDB-T symbol comprises 13 OFDM segments, with each segment occupying a bandwidth of 428.6 kHz (6/14 MHz). When 13 active segments are used, the total useful bandwidth is 5.57 MHz.

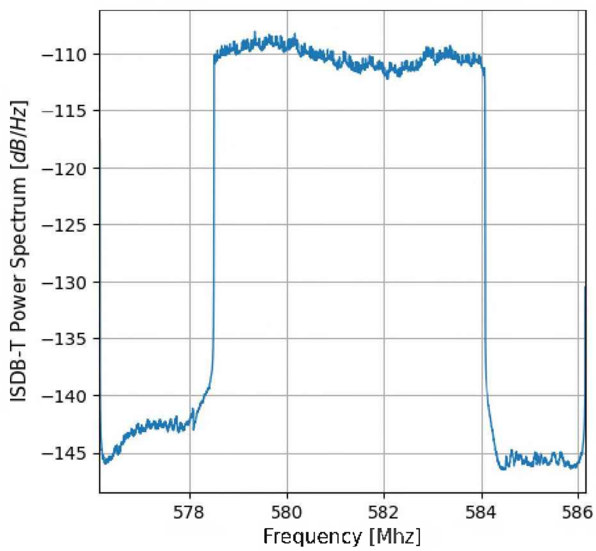

Fig. 3. Power spectrum of ISDB-T opportunity signal from Tv Universidad

The spectrum of the opportunity signal transmitted by TV Universidad, with a carrier frequency of 581.143 MHz, is depicted in Figure 3. The transmission mode is number three, featuring 5617 active carriers, and with an approximate bandwidth of 6 MHz. Some of the carriers are pilots employed for channel estimation and transmission control information. These produce unwanted deterministic peaks that affect the detection capabilities of the system.

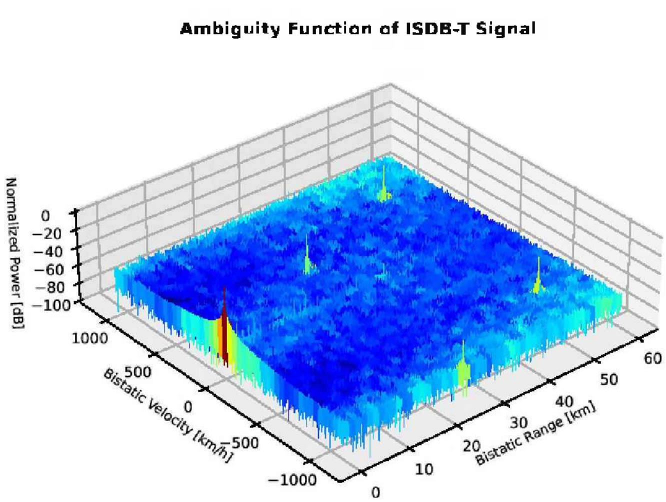

Fig. 4. Ambiguity Function of the opportunity signal

Figure 4 shows the Ambiguity Function of the opportunity signal. The calculation procedure is similar to (9), where the illuminator signal is correlated with the time and Doppler-shifted copy of itself. Deterministic peaks appear from 25 km of bistatic radar. This suggests that reference signal conditioning may not be strictly necessary in the short-range case.

III. Experimental Setup

In this section we describe the PBR system setup configuration and provide a preliminary evaluation of the expected coverage.

A. Setup Configuration

The PBR system setup consists of two 8th element Yagi-Uda antennas co-located on the roof of the Electrical Engineering Department. One antenna is aligned with the transmitter of opportunity, while the other points towards the surveillance area. To improve SNR and achieve a better noise figure, an LNA is added to the surveillance branch antenna. To preserve phase coherence between receiver channels, a signal generator and a Wilkinson power divider are employed for phase-shift calibration. The two subsystems are interconnected through a 4x2 RF switch, enabling the selection of either antenna signal acquisition or calibration signal as needed. The output of the RF switch is then connected to each channel of the USRP.

To achieve a broad frequency range, the SBX-120 daughterboard is chosen, allowing the center frequency to be set between 400 MHz and 4.4 GHz. The entire system is controlled using a Python code, providing efficient management and control during the experiments.

Additionally, the power supply and switching operations are managed using the GPIO ports of the USRP. The architecture scheme of the PBR system is depicted in Figure 5, while the roof where the antennas were co-located and the transmitter tower can be observed is shown in Figure 6.

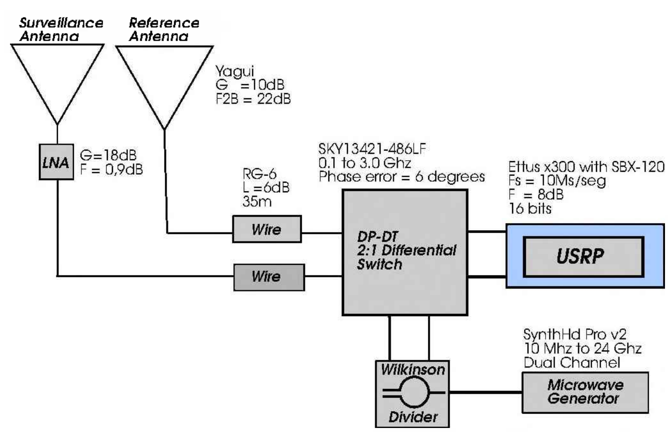

Fig. 5. Schematic of the PBR receiver.

The data reception routine begins with ensuring communication with the devices, followed by the validation of user input. Next, the calibration signal is acquired, and the phase shift is estimated. Subsequently, the PBR signals are obtained, and the routine awaits a new reception. This systematic process ensures a well-organized and efficient data acquisition sequence.

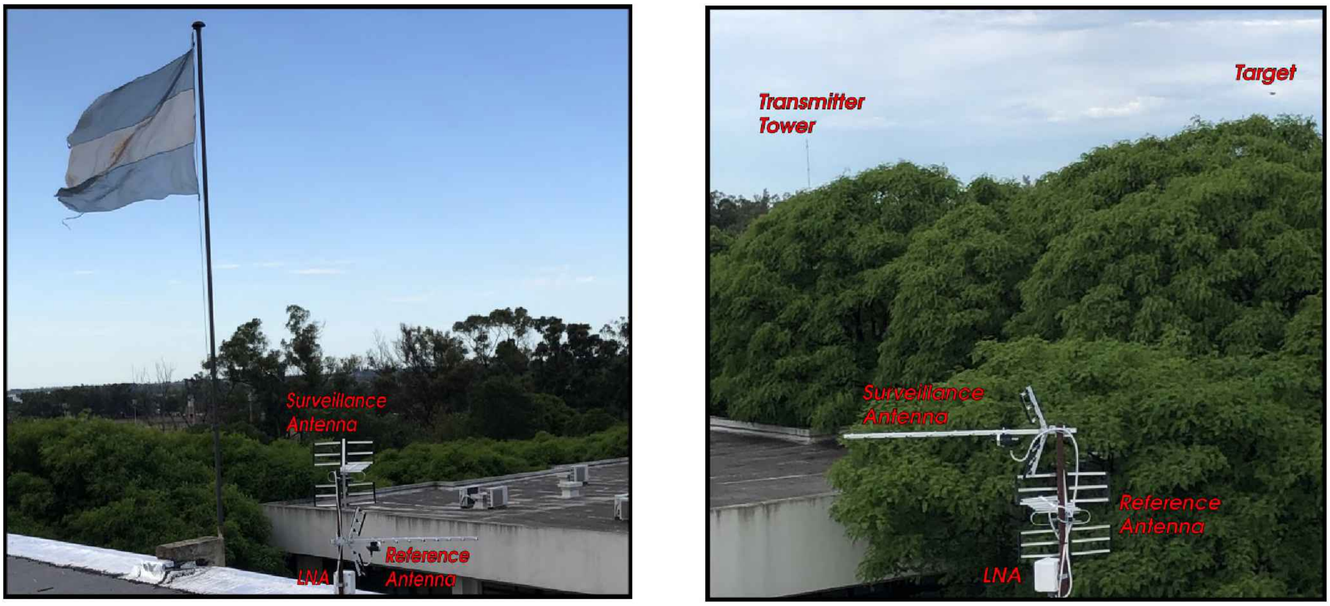

Fig. 6. Pictures showing components of the PBR system, which include antennas, LNA, and transmitter tower

B. Performance Prediction

The PBR utilizes the TV Universidad transmitter located in Berisso, approximately 2.4 km from the receiver. To ensure a relatively strong power of the reflected signal, it is recommended to select a measurement site where the moving target passes close to the receiver antenna.

Thus, the surveillance area was determined by considering the criteria of maximum direct path cancellation, avoiding interference from strong buildings, and aligning with the airway between La Plata Airport (SADL) and Ensenada Flying Club (PTL).

TABLE I
OPERATIONAL PARAMETERS OF THE PBR

Parameters	Value
Transmitter Power (P_T)	1 kW
Transmitter Antenna Gain (G_T)	0 dB
Receiver Antenna Gain (G_R)	10 dB
Wavelenght (λ)	0.51 m
Aircraft target RCS (σ_B)	$20m^2$
Helicopter target RCS (σ_B)	$3m^2$
Airplane altitude ($z(t)$)	4000 m
Helicopter altitude ($z(t)$)	1000 m
System Noise Figure (F_n)	2 dB
Baseline (L)	2.4 km
Coherent Processing Gain (G_{int} @ $T_{int} = 0.1s$)	60 dB
Receiver Bandwidth (B_R)	10 Mhz

To prepare the experiment and estimate the expected results based on detection theory, a power budget analysis is presented below. The well-known bistatic radar eq. (5) and the SNR for a given target eq. (6) are used. Table I includes all the other definitions and values adopted for the parameters listed in it.

The numerical values and bistatic radar geometry have been selected to be either identical or closely resembling those used in the experimental tests reported in the subsequent sections.

Figures 7 illustrates the expected SNR map across the surveyed area for an airplane target (RCS = $20m^2$) and a helicopter target (RCS = $3m^2$). The altitudes considered for the airplane and helicopter targets are 4000 meters and 1000 meters, respectively. The receiver, denoted as R_X, serves as the origin of the axes, and the transmitter position, denoted as T_X, is located at coordinates $(x_t, y_t) = (0.632, 2.324)$ km.

Based on PBR detection theory [7], achieving a probability of detection (p_d) of at least 95% with a probability of false alarm (p_{fa}) of 10^{-4} requires an SNR of approximately 24 dB. Notably, for the helicopter target scenario, this SNR value can be achieved at a distance of approximately 20 km from the PBR sensor, while in the case of an aircraft target, the SNR can be achieved around 30 km away. These findings demonstrate the system's capability to detect targets at considerable distances under the specified conditions.

It should be emphasized that this theoretical analysis does not consider the interference signals effects such as the direct signal from the transmitter and the returns from the stationary scene. The analysis assumes ideal conditions where these contributions have been perfectly removed by dedicated signal processing stages, allowing a noise-limited condition to be restored.

IV. RESULTS

In this section, we present the experimental test conducted on July 2023. We outline the signal processing scheme and

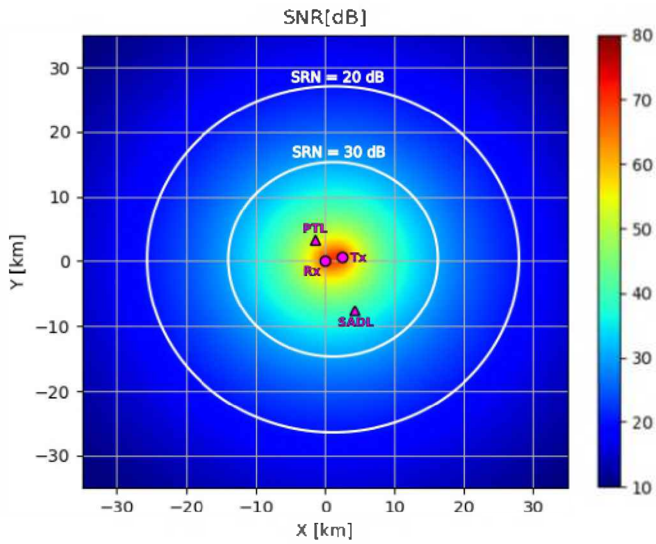

a) Helicopter at 1000m of altitude

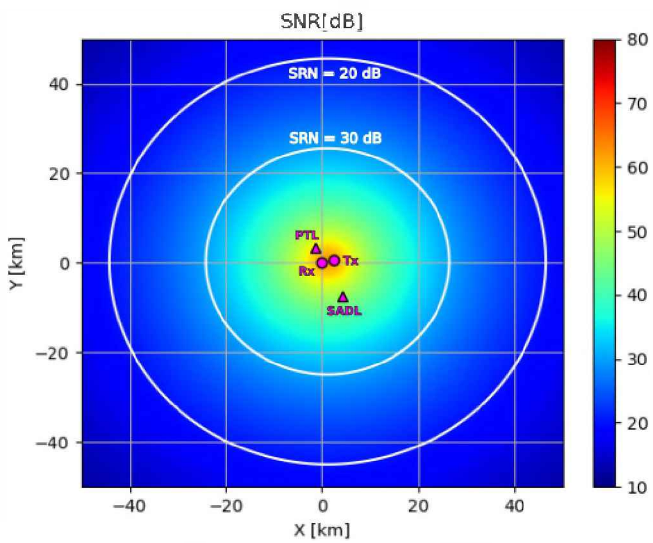

b) Airplane at 4000m of altitude

Fig. 7. Theoretical SNR for different targets and altitude from the PBR. The processing gain is 60 dB

present the results. Additionally, we compare the obtained results with those from a flight tracking service (ADS-B) [8],[9].

A. Acquisition Scenario

Several non-commercial aircrafts typically overfly the surveilled area without a known flight plan (useful for acquisition planning) and ADS-B system. Therefore, while numerous acquisitions were made, only a few could presently be verified. Two Airbus H125 helicopters were observed flying in formation at low altitudes near the Electrical Engineering building. Visual contact was made with them, but the location system was activated only on the last of the helicopters, making it impossible to accurately verify the separation between them.

The phase shift between channels is estimated with a second-long acquisition from the generator, followed by a 20-second antenna measurement. The processing routine is subsequently ran offline to analyze the acquired data.

B. Process Routine

The removal of the undesired contribution in the surveillance channel, i.e., the direct signal, clutter, and multipath echoes, is performed in the first step. The batch version of the extensive cancellation algorithm (ECA-B) [10] is employed for this purpose. The ECA-B operates by subtracting, from the surveillance signal, delayed replicas of the reference signal properly weighted, according to adaptively estimated coefficients. The filter weights are estimated and applied over smaller portions (batches) of the integration time. Batches T_B of small dimension are adopted to synthesize a wide Doppler cancellation notch. The ECA-B approach operates over a range of 6 km with a batch duration of $T_B = 0.04$s.

After the clutter cancellation stage, the output signals are used to evaluate the bistatic range-velocity map. For this purpose, CAFs were calculated using the Batches approach described in [4]. The concept is similar to the one used for clutter removal, where the integration time is divided into small batches for correlation calculation, resulting in reduced computational effort. The length of the batches were $T_B = 0.2s$, corresponding to $\Delta v \approx 9.3$ of km/h (size of the velocity bin).

C. Detection Plots

Figure 8 displays the 2-D range-velocity plots of the helicopter detections near the receiver. In the figure, the correlation peak appears at approximately 0.5 to 2 km of bistatic range, and the bistatic velocity measured is between 200 to 300 km/h. Additionally, some low-power peaks are observable, which were not canceled by the clutter filter and also the Doppler spread of the blades (vertical dots).

For ground-truth comparison, we calculated the bistatic parameters using equations (1), (2), (3), (4), and the flight data parameters provided by [8]. Figure 9 displays the bistatic range and the bistatic velocity versus time of the second helicopter in line. We can observe that the values correspond to the results obtained in the range-velocity map, demonstrating the capacity of the system to detect targets.

V. Conclusion and Future Work

The first section introduced the fundamental operation of PBR and covered the basics of the geomerty and signal processing, laying the foundation for the subsequent sections.

The second section focused on the system setup, emphasizing the crucial phase-shift correction that was performed to ensure coherent reception. This step was essential for accurate and reliable target detection. Also, a thorough power budget analysis was conducted, demonstrating the system's capability for target detection.

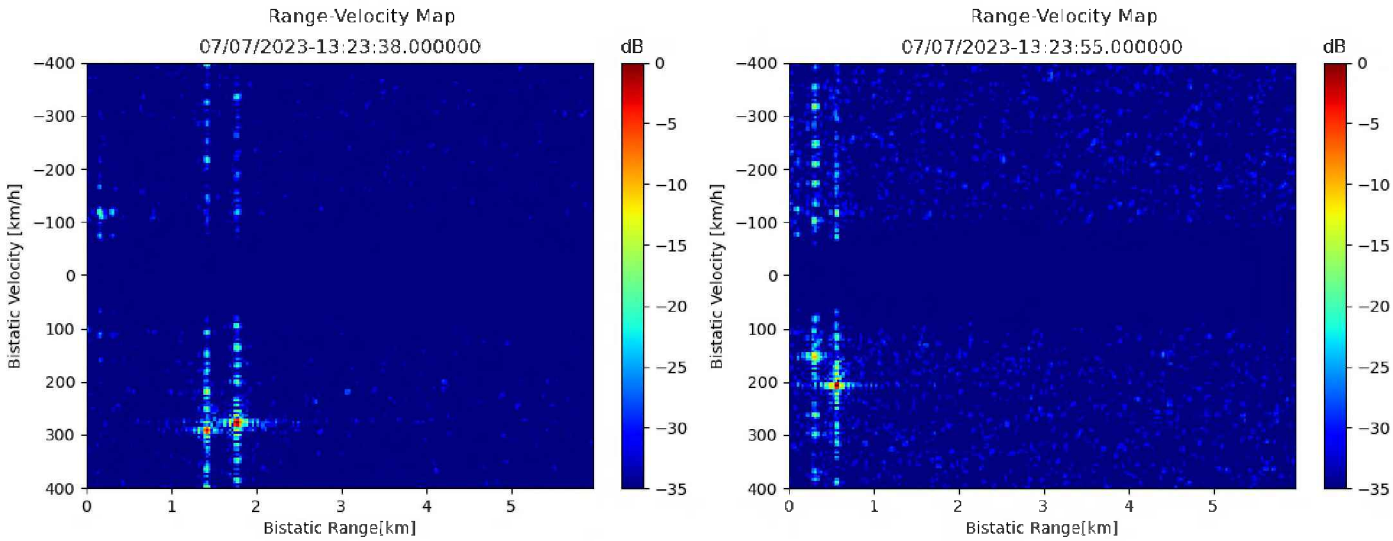

Fig. 8. 2-D Range-Velocity detection map of two helicopters flying in formation

Finally, a delay-doppler map analysis was presented, showcasing the obtained range-velocity plots of the detected targets. The comparison with ground-truth data further validated the system's performance in detecting targets at considerable distances.

Overall, the implementation of the PBR testbed using an USRP proved to be successful, and the real experimental results confirmed the system's effectiveness in target detection and ranging. Further improvements and future work may involve cleaning the reference to avoid the deterministic peaks, and the exploration of additional signal processing techniques to enhance the system's capabilities.

ACKNOWLEDGMENT

The authors are supported by CIC-PBA, CONICET, UNLP and by the following grants: UNLP I+D 11-I-257 and CONICET PIP-1515.

REFERENCES

[1] N. Willis, *Bistatic Radar*. Artech House radar library, Institution of Engineering and Technology, 2005.

[2] H. Griffiths and C. Baker, *An Introduction to Passive Radar, Second Edition*. Artech House radar library, Artech House, 2022.

[3] W. Feng, J. Friedt, G. Cherniak, and M. Sato, "Passive bistatic radar using digital video broadcasting–terrestrial receivers as general-purpose software-defined radio receivers," *Review of Scientific Instruments*, vol. 89, p. 104701, 10 2018.

[4] M. Malanowski, *Signal Processing for Passive Bistatic Radar*. Artech House radar library, Artech House, 2019.

[5] "About usrp bandwidths and sampling rates." https://kb.ettus.com/About_USRP_Bandwidths_and_Sampling_Rates, 2016. [Online; accessed July-2023].

[6] M. Takada and M. Saito, "Transmission system for isdb-t," *Proceedings of the IEEE*, vol. 94, no. 1, pp. 251–256, 2006.

[7] M. Conti, C. Moscardini, A. Capria, and R. Soleti, "Estimation of passive bistatic radar detection probability: Experimental results," 10 2014.

[8] "Flightradar24," 2022. https://www.flightradar24.com/ [Online; accessed July-2023].

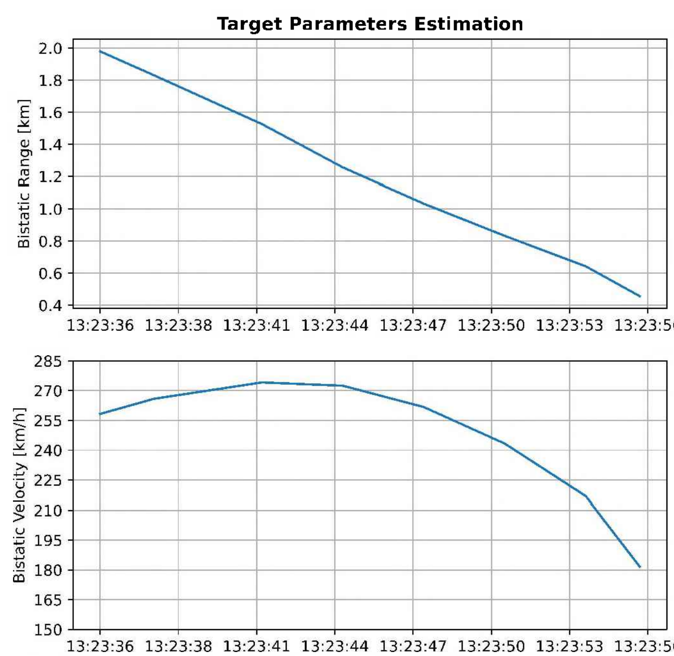

Fig. 9. Parameters of the second helicopter in line obtained using flight tracking service

[9] M. Varga, Z. A. Polgár, and H. Hedeşiu, "Ads-b based real-time air traffic monitoring system," in *2015 38th International Conference on Telecommunications and Signal Processing (TSP)*, pp. 215–219, 2015.

[10] F. Colone, D. W. O'Hagan, P. Lombardo, and C. J. Baker, "A multistage processing algorithm for disturbance removal and target detection in passive bistatic radar," *IEEE Transactions on Aerospace and Electronic Systems*, vol. 45, no. 2, pp. 698–722, 2009.